Supporting Information

An Acceptor with the Asymmetric and Extended Conjugated Backbone for High Efficiency Organic Solar Cells with Low Nonradiative Energy Loss

Jing Wang[a], Hongbin Chen[b], Xiaoyun Xu[c], Zaifei Ma[c]*, Zhe Zhang[b], Chenxi Li[b], Yang Yang[d], Jian Wang[d], Yue Zhao[e], Mingtao Zhang[b], Xiangjian Wan[b], Yan Lu[a]*, and Yongsheng Chen[b]*

[a] *School of Materials Science & Engineering, Tianjin Key Laboratory for Photoelectric Materials and Devices, Key Laboratory of Display Materials & Photoelectric Devices, Ministry of Education, Tianjin University of Technology, Tianjin 300384, China*

[b] *State Key Laboratory of Elemento-Organic Chemistry, The Centre of Nanoscale Science and Technology and Key Laboratory of Functional Polymer Materials, College of Chemistry, Renewable Energy Conversion and Storage Center (RECAST), Nankai University, Tianjin 300071, China.*

[c] *State Key Laboratory for Modification of Chemical Fibers and Polymer Materials, Center for Advanced Low-dimension Materials, College of Materials Science and Engineering, Donghua University, Shanghai 201620, China.*

[d] *The Institute of Seawater Desalination and Multipurpose Utilization, Ministry of Natural Resources (Tianjin), Tianjin 300192, China*

[e]*Coordination Chemistry Institute, State Key Laboratory of Coordination Chemistry, School of Chemistry and Chemical Engineering, Nanjing National Laboratory of Microstructures, Nanjing University, Nanjing 210093, China*

Correspondence to: mazaifei@dhu.edu.cn (Z.M.) luyan@tjut.edu.cn (Y.L.); yschen99@nankai.edu.cn (Y.C.)

1. Experimental section

1.1 Materials and synthesis

Donor polymer PBDB-TF (PM6) was synthesized by our group. 2-(5,6-difluoro-3-oxo-2,3-dihydro-1H-inden-1-ylidene)malononitrile (INCN-2F) was purchased from woerjiming (Beijing) Technology Development Institute. The main chemicals and super dry solvents were purchased from TCI chemical Co, J&K chemical Co, Alfa Aesar chemical Co and used without further purification. Other reagents and solvents were purchased from local suppliers. Detailed synthetic route of NQF were presented in Scheme S1.
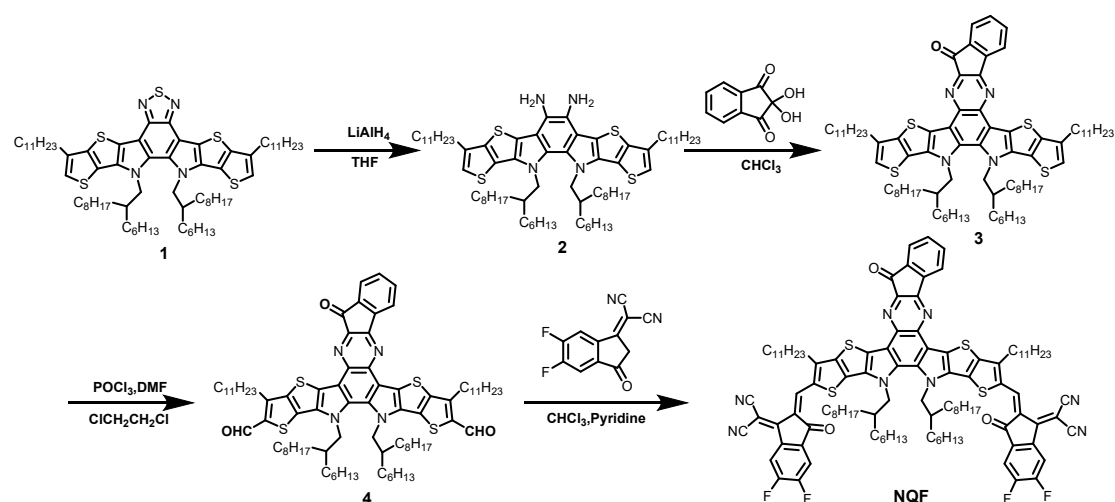
Scheme S1. Synthetic routes for NQF.

1.2 Synthesis of NQF

Synthesis of compound 3: LiAlH$_4$ (72 mg, 1.92 mmol, 5.0 eq.) was added to a 100 mL two-necked round bottom flask. Then the mixture was put in ice bath and degassed for three times and protected with argon gas. After that, compound **1** (460 mg, 0.385 mmol, 1.0 eq.) dissolved in 50 mL super dry tetrahydrofuran (THF) was added to the above mixture. The mixture was stirred and refluxed for 12 h. After being cooled to 0 °C, water (20 mL) is slowly dropped into the reaction and extracted with ethyl acetate. The organic layer was dried over anhydrous Na$_2$SO$_4$. After removal of solvent, the crude product was dissolved in dry chloroform (30 mL), and then 2,2-dihydroxyindane-1,3-dione (342 mg, 1.92 mmol, 5.0 eq.) was added to the solution.

The reaction was stirred at room temperature for 4-6 h, then the solvent was removed under vacuum. Finally, the crude product was purified by silica gel employing petroleum ether /CH_2Cl_2 (3:1 v/v) as an eluent to obtain compound **3** as a brown red solid (200 mg, 40%). ^1H NMR (400 MHz, CDCl$_3$, δ) δ 8.18 (d, J = 7.0 Hz, 1H), 7.86 (d, J = 6.9 Hz, 1H), 7.68 (t, J = 6.8 Hz, 1H), 7.47 (t, J = 6.8 Hz, 1H), 7.04 (s, 2H), 4.80-4.55 (m, 4H), 3.00-2.72 (m, 4H), 2.28-2.09 (m, 2H), 1.99-1.81 (m, 4H), 1.48-0.88 (m, 86H), 0.81-0.68 (m, 6H). ^{13}C NMR (400 MHz, CDCl$_3$) ^{13}C NMR (101 MHz, CDCl$_3$) δ 190.8, 155.5, 144.6, 144.3, 143.7, 142.4, 138.3, 137.9, 137.1, 136.8, 136.1, 136.0, 135.8, 135.3, 132.8, 131.1, 130.7, 124.2, 123.6, 123.2, 122.5, 121.6, 119.6, 119.5, 119.4, 118.5, 55.1, 55.0, 38.65, 31.9, 31.6, 30.5, 30.4, 30.3, 29.8, 29.7, 29.7, 29.6, 29.6, 29.6, 29.5, 29.4, 29.4, 29.2, 29.2, 29.0, 28.9, 25.5, 22.7, 22.6, 22.6, 22.5, 14.2, 14.1, 14.0.

Synthesis of compound 4: Compound 3 (200 mg, 0.148 mmol) and 40 mL super dry 1, 2-dichloroethane (ClCH$_2$CH$_2$Cl) were added to a 100 mL two-necked round bottom flask, then the super dry N, N-Dimethylformamide (DMF, 0.4 mL) was added to above mixture. The mixture was put in ice bath, then it degassed for three times and protected with argon gas. The mixture was stirred and refluxed for 12 h, then it was cooled to 0 °C. The mixture was slowly added 20-30 mL saturated sodium acetate solution and stirred at room temperature for 2 h. Then it was extracted with dichloromethane and the organic layer was dried over anhydrous Na$_2$SO$_4$. After removal of solvent, the crude product was purified by silica gel employing petroleum ether/CH_2Cl_2 (1:1 v/v) as an eluent to obtain compound 4 as an orange red solid. (150 mg, 75%). ^1H NMR (400 MHz, CDCl$_3$) δ 10.16 (s, 1H), δ 10.15 (s, 1H), 8.14 (d, J = 7.1 Hz, 1H), 7.85 (d, J = 7.0 Hz, 1H), 7.71 (t, J = 6.9 Hz, 1H), 7.47 (dd, J = 38.7, 31.9 Hz, 1H), 4.97-4.53 (m, 4H), 3.42-3.09 (m, 4H), 2.28-2.05 (m, 2H), 2.05-1.80 (m, 4H), 1.50-1.23 (m, 50H), 1.12-0.95 (m, 30H), 0.87-0.80 (m, 6H), 0.78-0.60 (m, 12H). ^{13}C NMR (101 MHz, CDCl$_3$) δ 190.1, 181.8, 181.8, 156.2, 147.0, 146.7, 145.4, 145.1, 144.6, 141.9, 137.8, 137.5, 137.2, 136.5, 136.0, 135.9, 135.6, 133.5, 131.7, 131.6, 129.5, 129.2, 127.3, 127.1, 124.4, 121.7, 120.0, 119.0, 55.4, 55.3, 38.9, 38.9, 31.9, 31.9, 31.8, 31.6, 30.7, 30.6, 30.5, 30.5, 30.4, 29.8, 29.7, 29.7, 29.6, 29.6, 29.6, 29.5,

29.4, 29.4, 29.3, 29.2, 29.2, 28.3, 28.2, 25.5, 22.7, 22.6, 22.5, 14.1, 14.1, 14.0.

Synthesis of NQF: Compound **4** (150 mg, 0.111 mmol, 1.0 eq.), 2-(5,6-difluoro-3-oxo-2,3-dihydro-1H-inden-1-ylidene)malononitrile (153 mg, 0.666 mmol, 6 eq.) and 30 mL dry $CHCl_3$ were added to a 100 mL two-necked round bottom flask, then the mixture was degassed for three times and protected with argon gas. After that, 0.4 mL super dry pyridine was added to the above mixture. The mixture was stirred and refluxed at 65 °C for 12 h. After being cooled to room temperature, the solvent was removed under vacuum. The crude product was then purified by silica gel employing petroleum ether/$CHCl_3$ (v/v = 1:3) as eluent to afford **NQF** as a blue black solid (140 mg, 71 %). ^{1}H NMR (400 MHz, $CDCl_3$) δ 9.12 (s, 1H), 9.06 (s, 1H), 8.60-8.40 (m, 2H), 8.04 (d, J = 7.3 Hz, 1H), 7.83 (d, J = 7.2 Hz, 1H), 7.77-7.65 (m, 3H), 7.54 (t, J = 7.4 Hz, 1H), 4.94-4.75 (m, 4H), 3.33-3.05(m, 4H), 2.40-2.19 (m, 2H), 1.98-1.73 (m, 4H), 1.64-1.46 (m, 5H), 1.45-0.93 (m, 75H), 0.86-0.82 (m, 6H), 0.79-0.66 (m, 12H). ^{13}C NMR (600 MHz, $CDCl_3$) δ 189.5, 186.1, 158.7, 156.6, 155.3, 155.2, 154.1, 153.8, 153.5, 153.5, 153.5, 153.4, 146.9, 145.8, 141.4, 138.4, 136.9, 136.6, 136.6, 136.0, 135.9, 135.9, 135.7, 135.1, 134.5, 134.3, 133.3, 132.7, 131.9, 131.8, 130.9, 130.6, 124.5, 121.8, 120.9, 119.9, 115.0, 114.8, 114.5, 114.5, 112.5, 112.4, 55.8, 55.7, 39.3, 39.3, 31.9, 31.9, 31.9, 31.9, 31.7, 31.7, 31.5, 30.8, 30.7, 30.7, 30.6, 30.0, 29.9, 29.9, 29.8, 29.7, 29.7, 29.7, 29.6, 29.6, 29.5, 29.4, 29.4, 29.3, 25.9, 25.8, 25.7, 25.7, 22.7, 22.6, 22.5, 22.5, 14.1, 14.1.

1.3 General characterization

The ^{1}H and ^{13}C nuclear magnetic resonance (NMR) spectra of compound 3, compound 4 were taken on a Bruker AV400 Spectrometer. The ^{1}H NMR spectra of NQF was taken on a Bruker AV400 Spectrometer and ^{13}C NMR spectra of NQF was taken on a Bruker AV600 Spectrometer. High resolution mass spectrums were performed on a Bruker solariXMRMS. UV-vis spectra were obtained with a Cary 5000 spectrophotometer.

1.4 Fabrication of OPV Devices

The conventional devices based on PM6:NFAs were fabricated with an architecture of indium–tin oxide (ITO)/poly(3,4-ethylenedioxythiophene):poly(styrene-sulfonate) (PEDOT:PSS)/active layer/2,9-bis[3-(dimethyloxidoamino)propyl]anthra[2,1,9-def:6-,5,10-d′e′f′]diisoquinoline-1,3,8,10(2H,9H)-tetrone (PDINO)/Ag. In detail, the ITO glass was pre-cleaned in turn in an ultrasonic bath of detergent, deionized water, acetone and isopropanol. Then the surface of ITO was treated by UV light in an ultraviolet-ozone chamber (Jelight Company) for 15 min. A thin layer of PEDOT:PSS (Baytron PVP Al 4083) was prepared by spin-coating the PEDOT:PSS solution at 4300 rpm for 20 s on the ITO substrate. Note that the PEDOT:PSS solution was pre-filtered through a 0.45 mm poly(tetrafluoroethylene) (PTFE) filter. Subsequently, the PEDOT:PSS films were baked at 150 °C for 20 min in air and transferred to a glove-box filled with argon. Then the PM6:NFAs mixtures were fully dissolved in chloroform (CF) with different ratios of 1-chloronaphthalene (CN) as additive at a concentration of 6 mg/mL of PM6 and the resulting solutions were spin-casted at 2000 rpm for 30 s onto the PEDOT:PSS layer. Thermal annealing was performed at 100 °C for 5 min. After that, about 10 nm thickness of PDINO (dissolved in methanol with the concentration of 2 mg/mL) layer was spin-coated on the top of the active layer. Finally, a layer of Ag with thickness of 150 nm was deposited under under 2×10^{-6} Pa. The active area of the device was 4 mm^2. The thickness of the active layers was about 120 nm which was measured by a Veeco Dektak 150 profilometer.

1.5 Single-crystal growth

Single crystals of **NQF** were grown by the liquid diffusion method at room temperature. In detail, 2 mL of methanol is transferred to 200 μL of concentrated chloroform solution of **NQF** slowly, and the beautiful acicular crystals were formed on the inner glassy tube after about 2-3 days. The X-ray diffraction signals of single crystals were collected on Bruker D8 Venture with metaljet. The crystal was kept at 173 K during data collection. The detailed crystal parameters were summarized in Supplementary **Table S1.**

1.6 CV experiments

Cyclic voltammetry (CV) experiments were performed with a LK98B II Microcomputer-based Electrochemical Analyzer in acetonitrile solutions. All measurements were carried out at room temperature with a conventional three-electrode configuration employing a glassy carbon electrode as the working electrode, a saturated calomel electrode (SCE) as the reference electrode, and a Pt wire as the counter electrode. Tetrabutylammonium phosphorus hexafluoride (n-Bu$_4$NPF$_6$, 0.1 M) in acetonitrile solution was used as the supporting electrolyte, and the scan rate was 100 mV s^{-1}. The highest occupied molecular orbital (HOMO) and lowest unoccupied molecular orbital (LUMO) energy levels were calculated from the onset oxidation potential and the onset reduction potential, using the equation $E_{\mathrm{HOMO}} = -(4.80 + E_{\mathrm{ox}}^{\mathrm{onset}})$, $E_{\mathrm{LUMO}} = -(4.80 + E_{\mathrm{re}}^{\mathrm{onset}})$.

1.7 DFT simulation

The geometry structures of NQF and Y6 were optimized by using DFT calculations (B3LYP/6-31G(d)), and the frequency analysis was followed to assure that the optimized structures were stable states. All calculations were carried out using Gaussian 16.

1.8 TEM measurement

The specimen for TEM measurement was prepared by spin casting the active

layer blend solution on ITO/PEDOT:PSS substrate, then floating the film on a water surface, and transferring to TEM grids. Transmission electron microscopy (TEM) was performed on a FEI-Tecnai G2 Spirit TWIN at 100 kV.

1.9 AFM measurement

Atomic force microscopy (AFM) images were performed using in tapping mode on a Bruker Dimension Icon atomic force microscope.

1.10 GIWAXS measurement

GIWAXS measurement was performed at Xeuss 2.0 SAXS/WAXS equipment. All samples were deposited on the silicon and were irradiated at a fixed X-ray incident angle of 0.2° with an exposure time of 1800 s.

1.11 Current density-voltage (*J-V*) and EQE measurement

The current density-voltage (*J-V*) characteristics of photovoltaic devices were recorded by a Keithley 2400 source-measure unit. The photocurrent was measured under illumination simulated 100 mW cm^{-2} AM1.5G irradiation using a Enli SS-F5-3A solar simulator, which was calibrated by a standard Si solar cell (made by Enli Technology Co., Ltd., Taiwan, and calibrated report can be traced to NREL). External quantum efficiency (EQE) values of the devices were measured using a QE-R Solar Cell Spectral Response Measurement System (Enli Technology Co., Ltd., Taiwan).

1.12 SCLC measurement

The hole and electron mobility were measured using the space charge limited current (SCLC) method, employing a diode configuration of ITO/PEDOT:PSS/active layer/Al for hole and ITO/ZnO/PFNBr/active layer/PDINO/Ag for electron by taking the dark current density in the range of 0-8 V and fitting the results to a space charge

limited form, where SCLC is described by:

$$J = \frac{9\varepsilon_0\varepsilon_r\mu_0 V^2}{8L^3}$$

where J is the current density, L is the film thickness of the active layer, μ is the hole or electron mobility, ε_r is the relative dielectric constant of the transport medium, ε_0 is the permittivity of free space (8.85×10^{-12} F m^{-1}), V (= V_{appl} - V_{bi}) is the internal voltage in the device, where V_{appl} is the applied voltage to the device and V_{bi} is the built-in voltage due to the relative work function difference of the two electrodes.

1.13 Electroluminescence measurement

Electroluminescence measurements were done using a source meter (Keithley 2400) to inject electric current, and the emitted photons were measured using a fluorescence spectrometer (KYMERA- 328I-B2, Andor technology LTD) with a Si EMCCD camera (DU491A-1.7, Andor). Injection current to the organic solar cell was 1 mA by direct current meter (PWS2326 Tectronix).

1.14 PL measurement

Photoluminescence measurements were taken using FLS1000 and emission spectra were obtained using the same setup used for recording electroluminescence spectra (Detector for NIR 5509 PMT, 600-1700 nm).

1.15 Sensitive EQE measurement

Sensitive EQE measurements were done using a halogen lamp light source, chopped at a frequency of 173 Hz, a monochromator (Newport CS260), a Stanford SR830 lock-in amplifier, a Stanford SR570 current amplifier, and a set of long pass filters. Lamp intensity was calibrated using a Si detector (Hamamatsu s1337-1010BQ). Transient photovoltage decay measurements were done using two green LEDs. One of the LEDs was used for constant bias illumination. The LED was driven by a Keithley 2450 with a varied injection current, for different bias illumination intensities. The other LED was driven by an arbitrary function generator (AFG3000)

purchased from Tektronix, at a pulse frequency of 500 Hz, a pulse width of 10 microseconds, for the voltage decay signal. The voltage signal from the solar cells was measured by an oscilloscope (MDO4104C) from Tektronix.

1.16 EQE$_{EL}$ measurements

EQE$_{EL}$ measurements were done using a home built setup using a Keithley 2400 to inject current to the solar cells. Emission photon-flux from the solar cells was recorded using a Si detector (Hamamatsu s1337-1010BQ) and a Keithley 6482 picoammeter.

1.17 Details for V$_{oc,rad}$ determination

$V_{oc,rad}$ is the V_{oc} when there is only radiative recombination in the OSC. The radiative recombination limit for the saturation current (J$_0$,rad) can be calculated from the EQEpv spectrum using the detailed balance theory:

$$J_{0,rad} = q \int EQE_{PV}(E) \emptyset_{BB}(E) dE$$

Wherein, q is the elementary charge, Φ_{BB} is the blackbody photo flux at 300K and E is the energy of the photons. EQEpv is obtained by attached the EQE spectrum determined from measured EL spectrum by use of reciprocity relation (EQE(E)=EL(E)* Φ_{BB}) to the measured sEQE spectrum, as shown in Figure 3(a-b). Then the V$_{oc, rad}$ is obtained from the following equation:

$$V_{oc,rad} = \frac{kT}{q} \ln \left(\frac{J_{ph}}{J_{0,rad}} \right)$$

Here, k is the Boltzmann constant, and Jph is the photocurrent density in the device under an open-circuit condition (assumed to be equivalent to the J_{sc}).

2. Supporting figures (Figure S1-Figure S16)
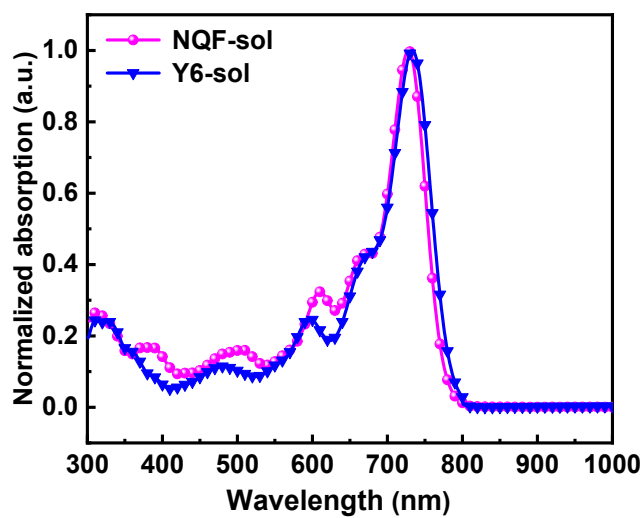
Figure S1. Normalized UV-Vis absorption spectra of NQF and Y6 in chloroform solutions.
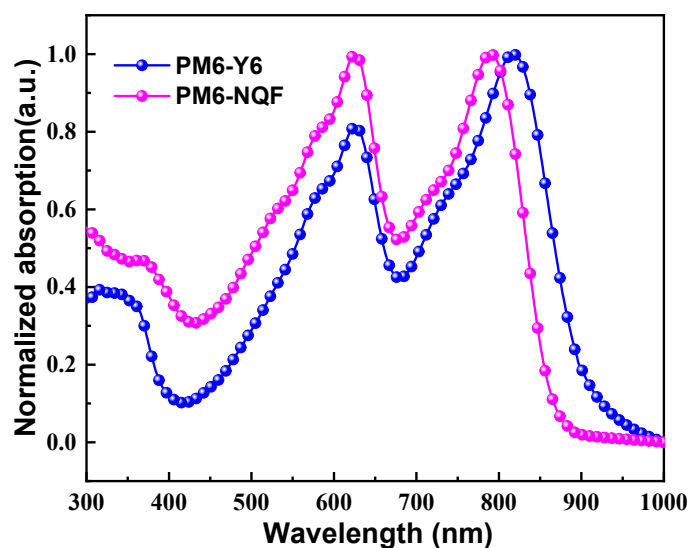
Figure S2. UV-vis absorption spectra of PM6:Y6 and PM6:NQF blend films under the same condition.
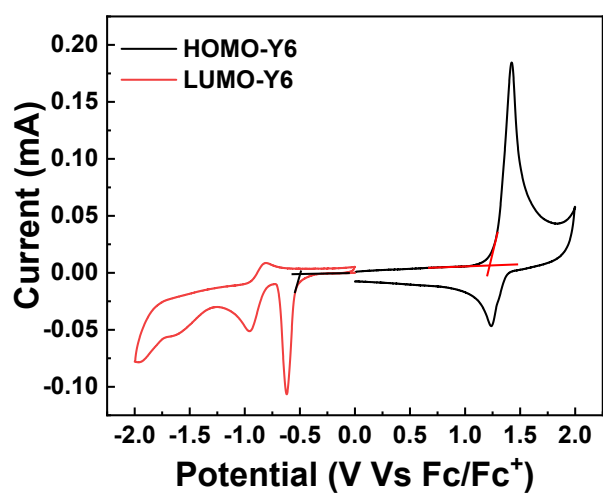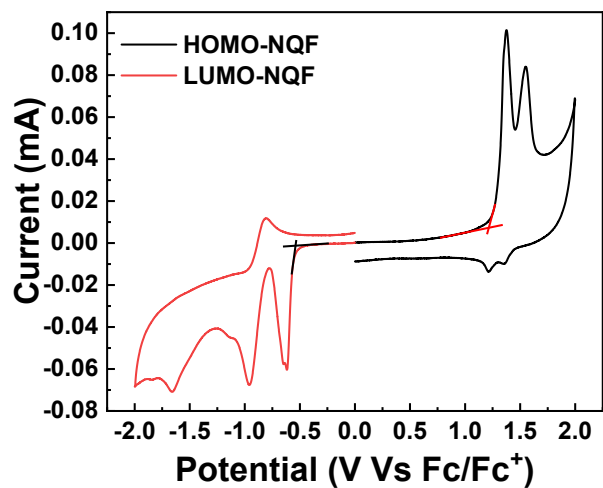
Figure S3. CV curves of NQF and Y6 in solid film state.
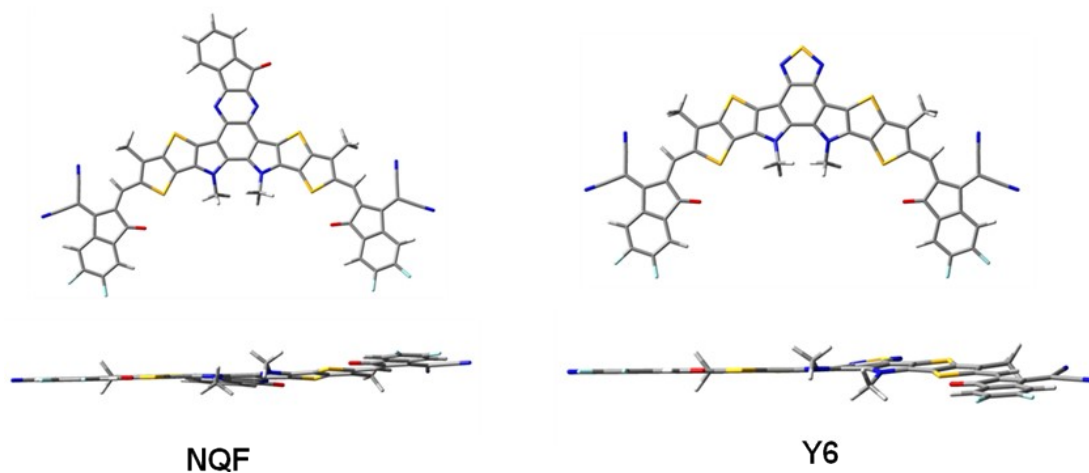
Figure S4. Chemical structures of NQF and Y6 and corresponding optimized molecular geometries at B3LYP/6-31G(d) level.
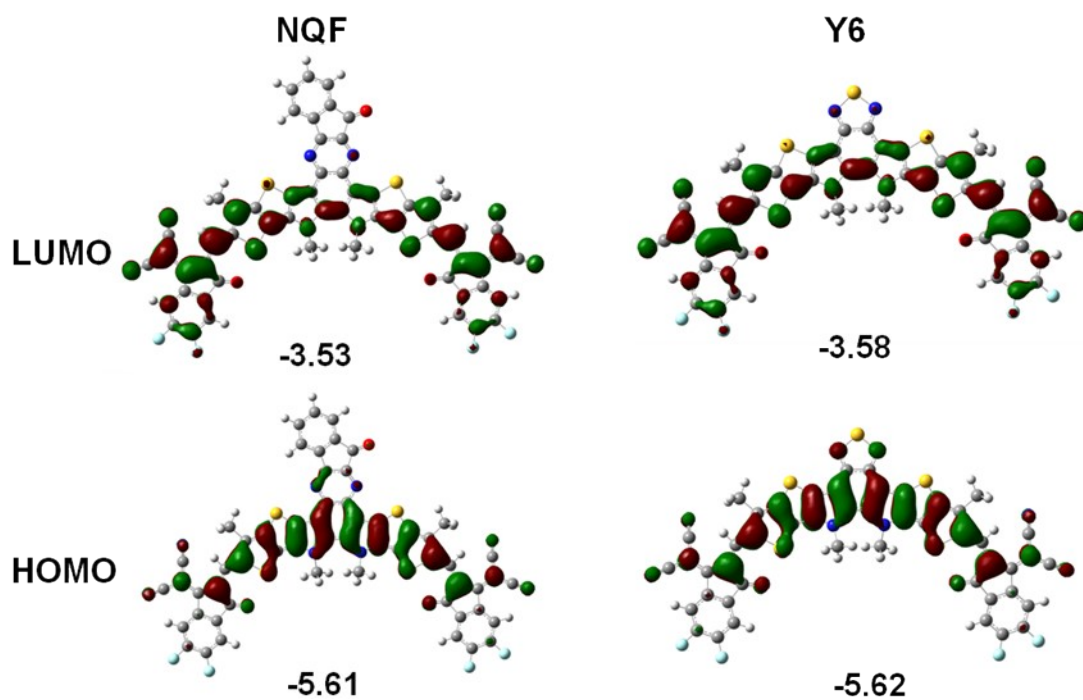
Figure S5. Theoretical density distribution for the frontier molecular orbitals via DFT-based theoretical calculations of NQF and Y6 at B3LYP/6-31G (d) level.
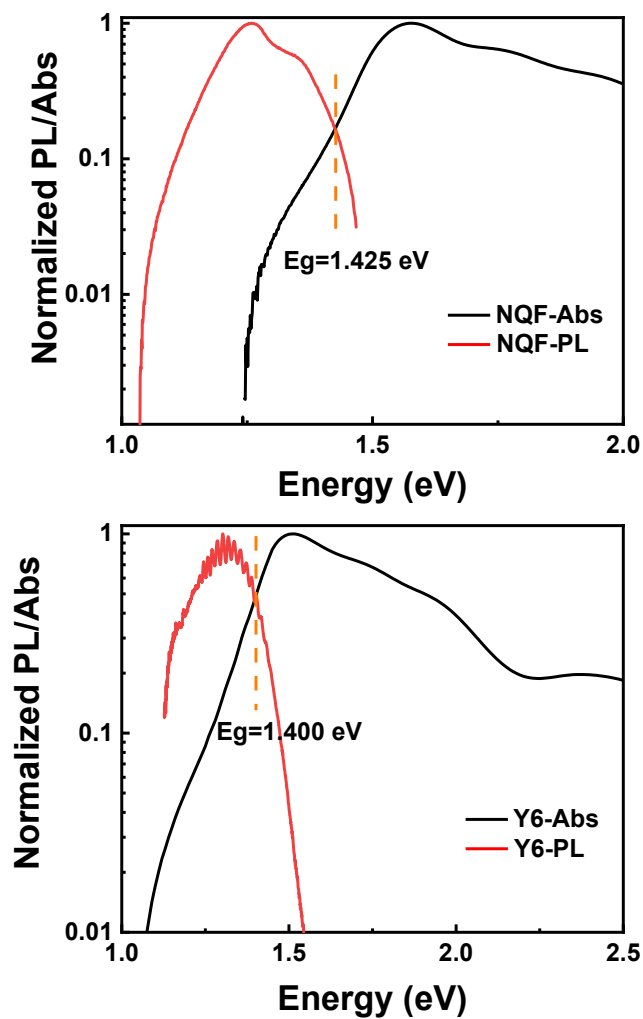
Figure S6. Normalized PL and UV-vis Abs spectra of low bandgap NQF and Y6 acceptors.

(a)
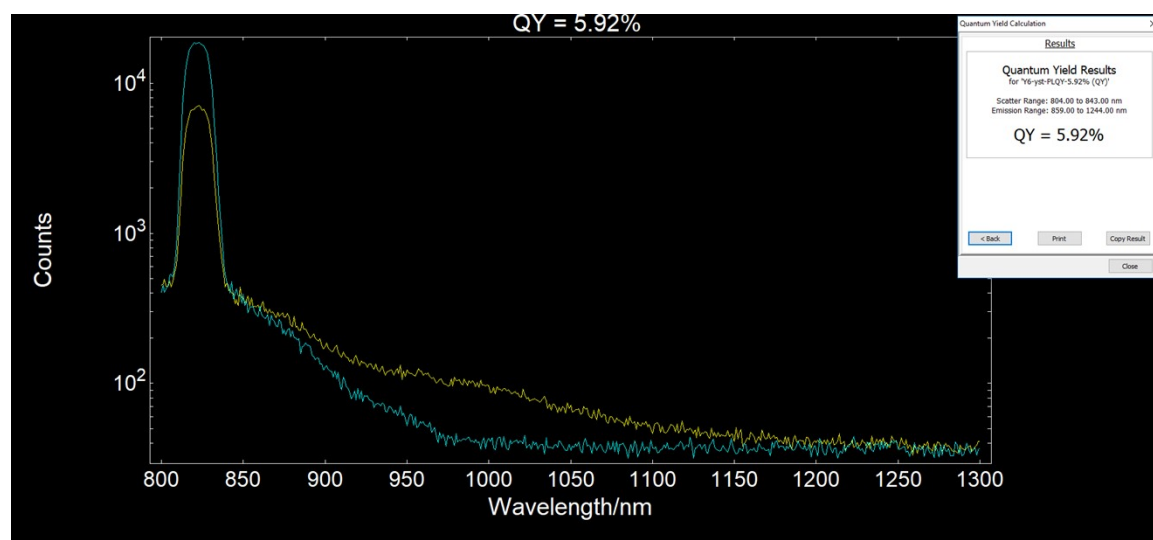
(b)
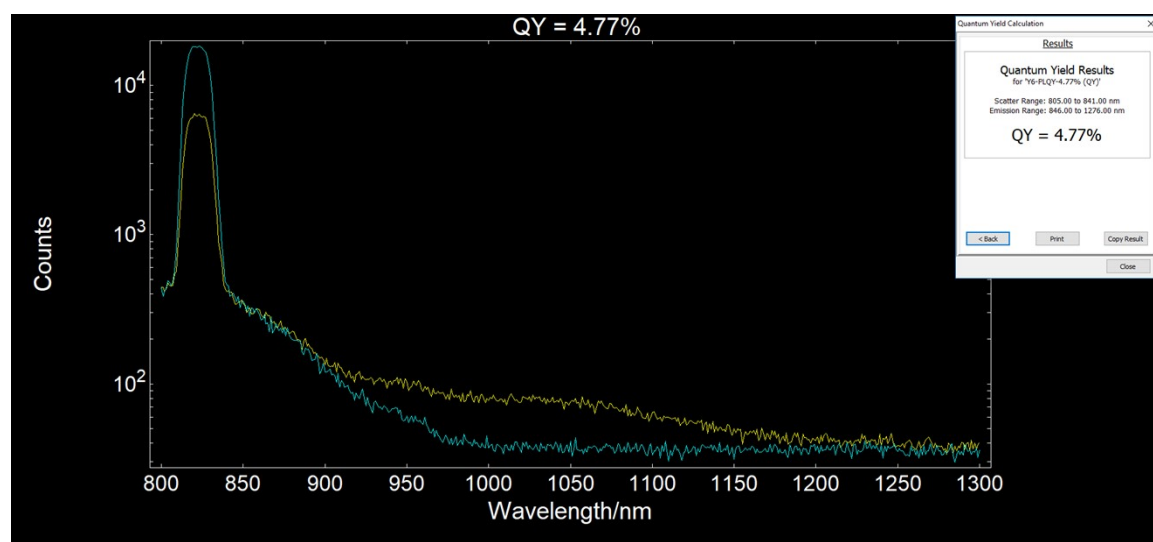
Figure S7. PLQY measurement of (a) NQF and (b) Y6.
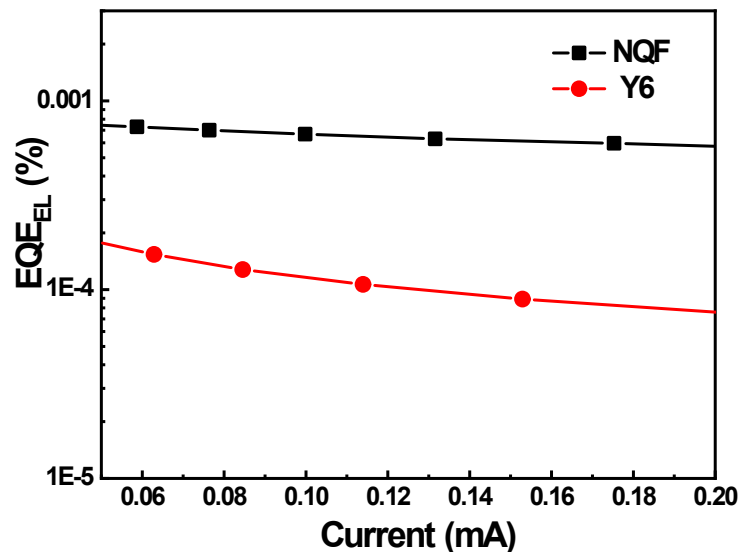
Figure S8. EQE_{EL} spectra of NQF pure phase device and Y6 pure phase device.
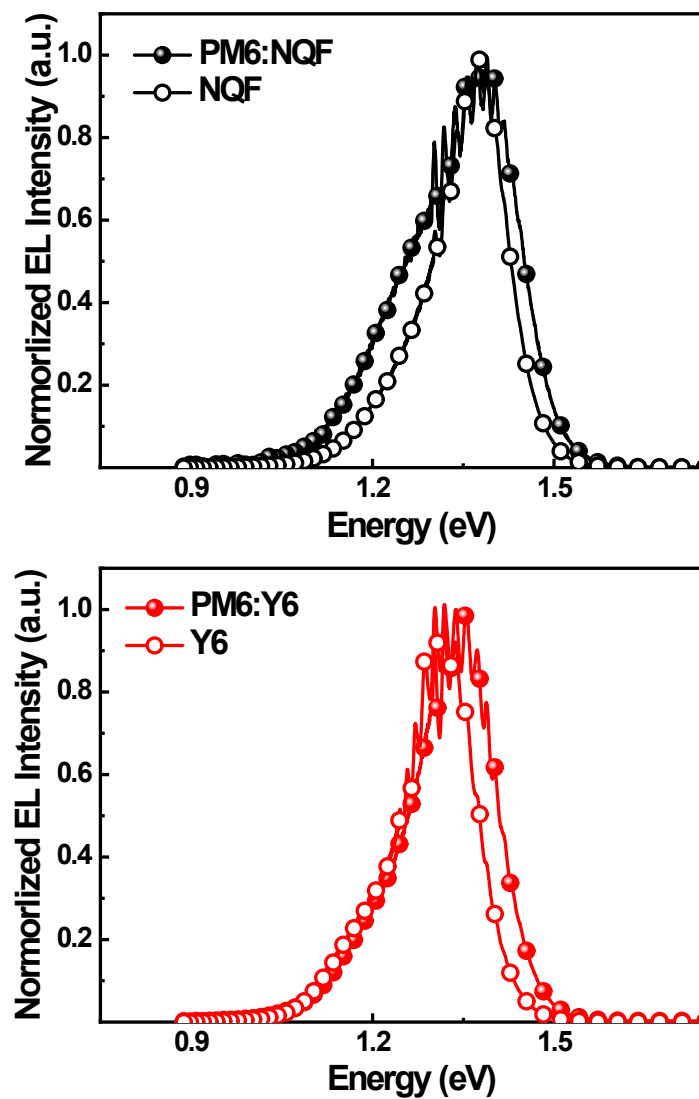
Figure S9. Normalized electroluminescence spectra (EL) curves of optimized PM6:NQF blend film device, NQF pure phase device and PM6:Y6 blend film device, Y6 pure phase device.
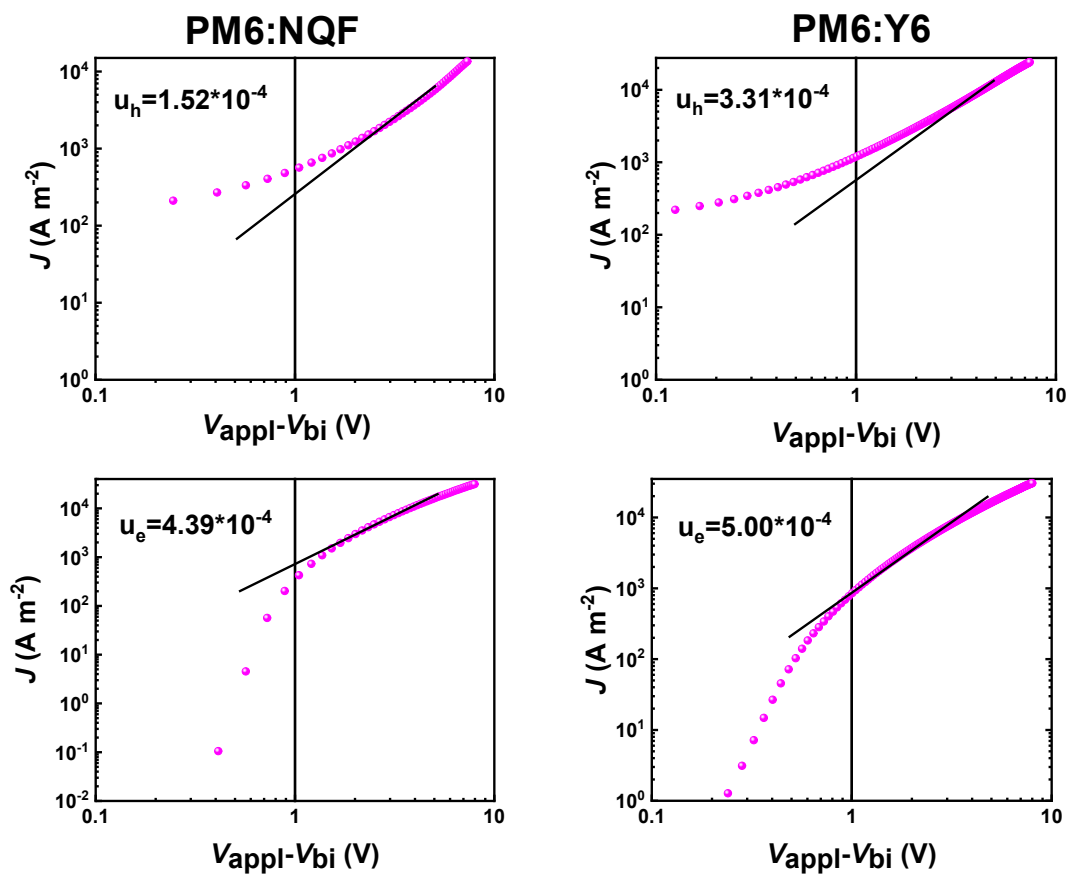
Figure S10. The current-density-voltage (*J-V*) plots for hole-only and electron-only devices based on PM6:NQF and PM6:Y6.
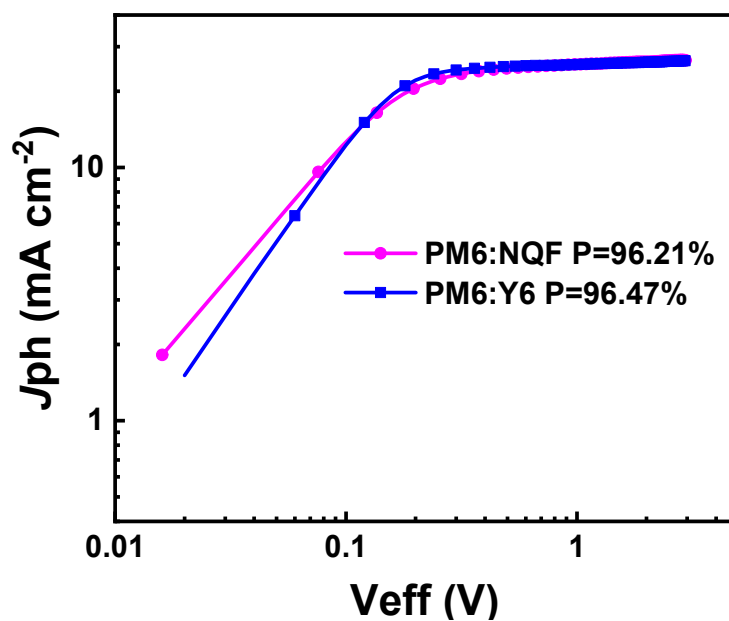
Figure S11. Effective voltage (V_{eff}) dependence of J_{ph} of for PM6:NQF based device and PM6:Y6 based device for the optimized devices.
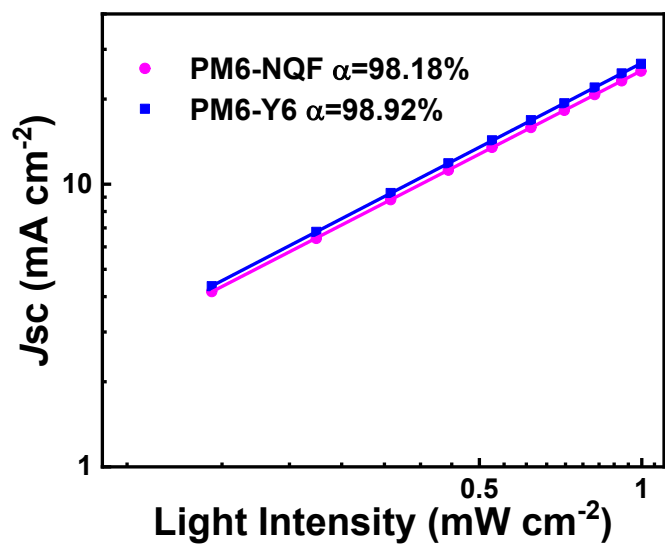
Figure S12. Light intensity (P) dependence of J_{sc} of for PM6:NQF based device and PM6:Y6 based device for the optimized devices.
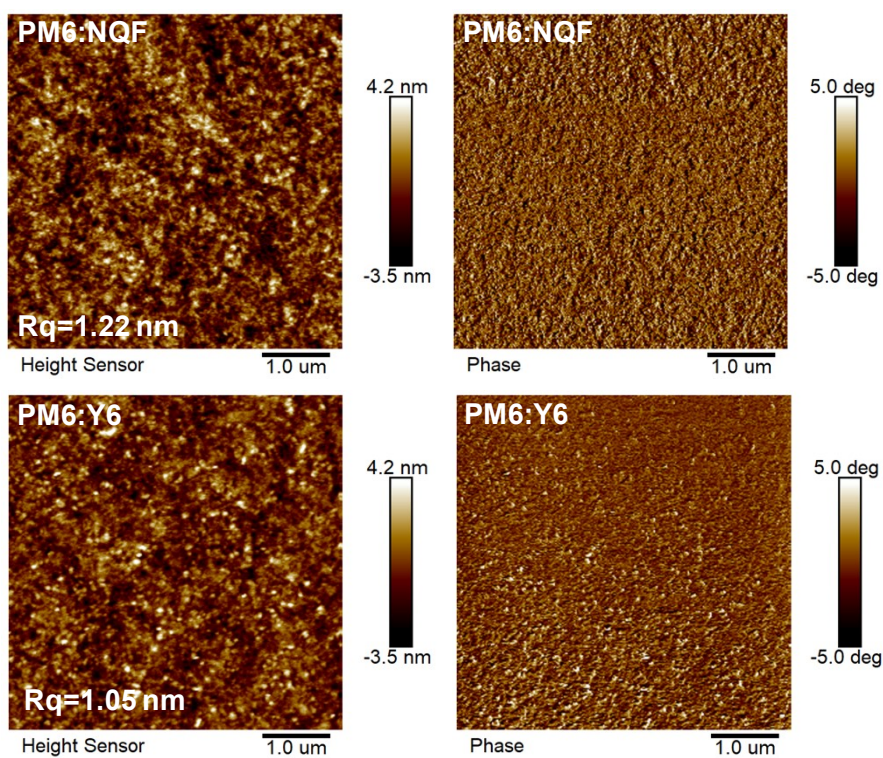
Figure S13. AFM images of optimized PM6:NQF and PM6:Y6 blend films.
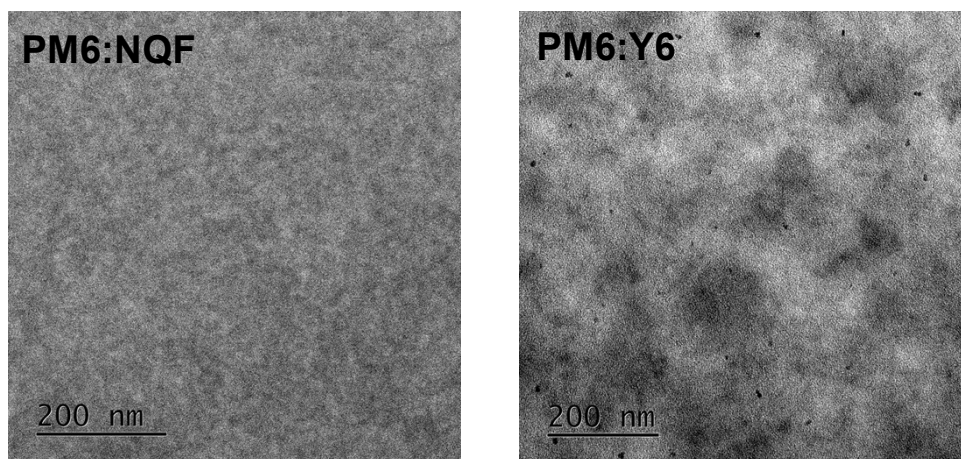
Figure S14. TEM images of optimized PM6:NQF and PM6:Y6 blend films.
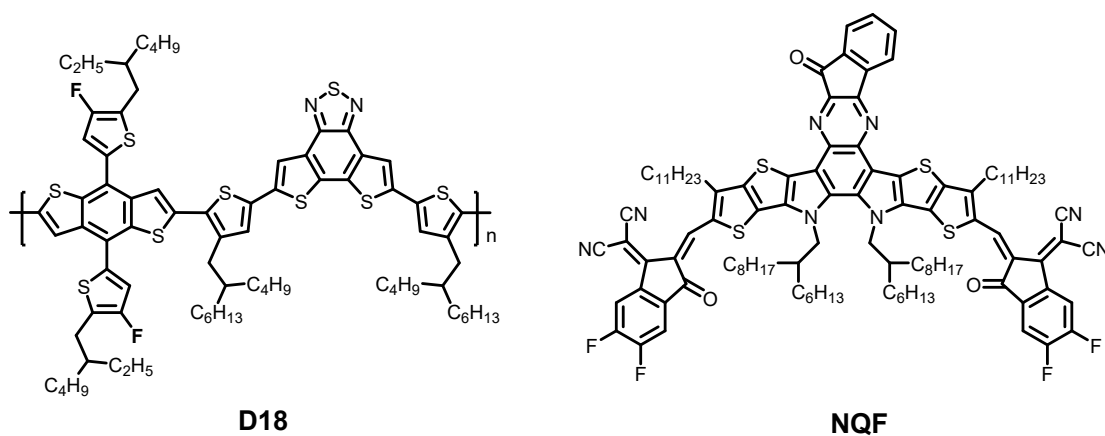
Figure S15. The chemical structure of D18 and NQF.
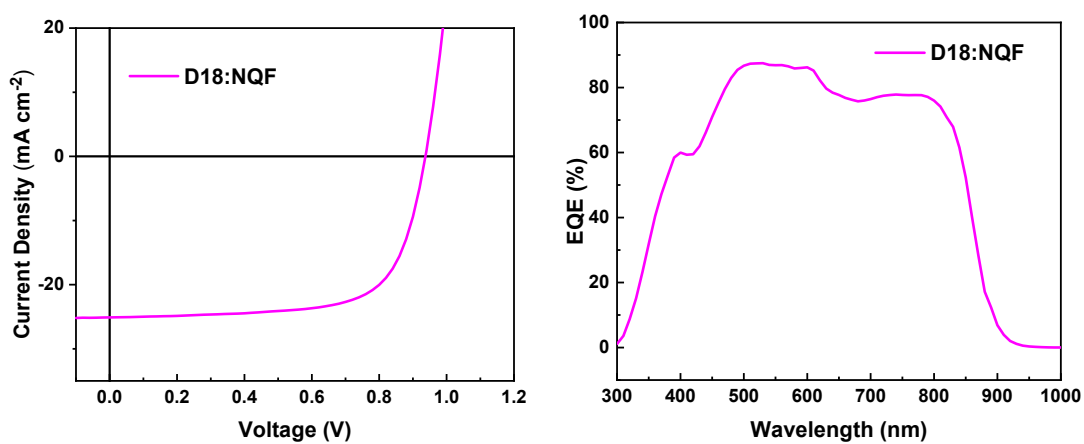
Figure S16. The *J-V* curves and EQE curves of the devices of D18:NQF.

3. Supporting tables (Table S1-S5)

Table S1. The solubility, electron mobilities of Y6 and NQF.

Films	*Solubility* (mg/mL)	μ_e (10^{-4} cm^2 V^{-1} s^{-1})
Y6[a]	**47.68**	**3.26**
NQF[a]	**389.26**	**5.53**

μ_e is electron mobilities of optimized blend film by SCLC measurements.

Table S2. Crystal data and structure refinement for NQF.

Comp: **NQF**	CCDC:2155815
Empirical formula	$C_{107}H_{122}F_4N_8O_3S_4$
Formula weight	1772.36
Temperature	173.00K
Crystal system	Ticlinic
Space group	P-1
Unit cell dimensions	a = 14.411(2) Å
	b = 19.397(3) Å
	c = 19.702(3) Å
	α/° = 107.665(5)
	β/° = 94.222(5)
	γ/° = 105.951(5)
Volume	4971.3(13) Å^3
Z	2
ρ calc	1.184 g/cm3
μ	0.889 mm^{-1}
F(000)	1888.0
Crystal size	0.13 × 0.12 × 0.1 mm3
Radiation	GaKα (λ = 1.34139)
2 θ range for data collection	4.916 to 107.81°
Index ranges	-17 ≤ h ≤ 17, -23 ≤ k ≤ 21, -23 ≤ l ≤ 23
Reflections collected	53095
Independent reflections	18131 [Rint = 0.0775, Rsigma = 0.0881]
Data / restraints / parameters	18131/402/1136
Goodness-of-fit on F^2	1.129
Final R indices [I>2σ(I)]	R_1 = 0.1417, wR_2 = 0.3255
Final R indexes [all data]	R1 = 0.2059, wR_2 = 0.3542
Largest diff. peak /hole	0.98/-0.72 e Å^{-3}

The X-ray diffraction signals of single crystals were collected on Bruker D8 Venture with metaljet at 173K.

Table S3. Detailed photovoltaic parameters of the PM6:NQF based devices processed by varied conditions under illumination of AM 1.5 G, 100 mW/cm^2.[a]

D/A [w/w]	CN [V/V]	Thermal annealing （TA） [°C]	V_{OC} [V]	J_{SC} [mA cm^{-2}]	FF [%]	PCE [%]
1:1	-	-	0.949	22.97	65.10	14.19
1:1.2	-	-	0.945	24.51	64.58	14.96
1:1.4	-	-	0.942	24.15	64.52	14.67
	-	100	0.909	26.05	63.70	15.08
1:1.2	-	110	0.909	25.91	66.75	15.77
	-	120	0.899	24.59	65.38	14.45
	0.3	-	0.934	23.14	69.09	14.93
1.1.2	0.5	-	0.939	24.51	71.92	16.55
	0.7	-	0.939	24.75	66.76	15.51
	0.5	100	0.920	24.98	73.80	16.96
1:1.2	0.5	110	0.921	25.79	73.96	17.57
	0.5	120	0.917	24.32	69.77	15.55

[a]The device architecture is ITO/ PEDOT:PSS /active layer/PDINO/Ag; D = 6 mg/mL in chloroform; 2000 rpm for 30 s.

Table S4. Summary of efficiency and nonradiative energy loss in recently reported binary OSCs.

Material system	ΔV_{nr} (V)	PCE_{max} (%)	Ref.
PM7：Y5	0.13	3.28	1
PBT1-C-2Cl:BTA3	0.16	3.9	2
BDT-ffBX-DT: SFPDI	0.22	6.2	3
PDCBT-2F: IT-M	0.21	6.4	4
BDT-ffBX-DT: PDI6	0.26	7.1	3
PTB7-Th: IEICO	0.23	7.2	4
BDT-ffBX-DT: PDI4	0.28	7.5	3
PffBT4T-2DT: $PC_{71}BM$	0.33	7.5	5
PffBT4T-2DT: FBR	0.23	7.8	5
PTB7-Th: $PC_{71}BM$	0.42	8.2	4
PBDB-T: $PC_{71}BM$	0.398	9.04	6
P3TEA: $SF-PDI_2$	0.26	9.5	7
PBDB-T: ITIC	0.37	9.9	8
PffBT4T-2DT: IDTBR	0.27	10.0	5
PBQ-QF: IEICO-4F	0.30	10.5	4
PBDB-T: ITIC	0.391	10.54	6
PBDB-T:SM-16	0.145	11.14	9
PBDB-T: IT-M	0.375	11.52	6
PMOT40: i-IEICO-4F	0.28	13.0	10
PM6: ANT-4F	0.22	13.1	11
PBDB-T: Y1	0.25	13.42	12
PBDB-T: Y2	0.26	13.4	12
PM6: ITC-2Cl	0.32	13.6	13
PM6: Y11(As-cast)	0.17	13.8	14
PM6:SN	0.15	14.4	15
PBDB-T:LL2	0.21	14.75%	16
PM6: BTP-eC7	0.225	14.9	17
PM6: BTP-S1	0.24	15.2	18
PM6: Y6	0.23	15.6	12
PM6: BTP-S2	0.22	16.4	18
PM6: Y11(annealing)	0.20	16.5	14
PM6: BTP-4Cl	0.21	16.5	12
PBDB-T:LL3	0.18	16.82%	16

PM6：NQF	**0.177**	**17.57**	**This work**
PM6: BTP-eC11	0.23	17.3	17
PM6: BTP-eC9	0.23	17.8	17
$\Delta V_{nr}= -kTln(EQE_{EL})$			

Table S5. A summary of d-spacing and coherence lengths (CL) of the samples.

Systems	Lamellar				π-π			
	q_r $[Å^{-1}]$	d^a $[Å]$	FWHM $[Å^{-1}]$	CL^b $[Å]$	q_z $[Å^{-1}]$	d^a $[Å]$	FWHM $[Å^{-1}]$	CL^b $[Å]$
NQF	0.3	20.94	0.097	58.30	1.73	3.63	0.342	16.53
	0.46	13.78	0.131	43.17				
Y6	0.29	21.67	0.078	72.50	1.76	3.57	0.235	24.06
PM6	0.29	21.67	0.084	67.32	1.65	3.80	0.247	22.89
PM6-NQF	0.3	20.94	0.061	92.70	1.72	3.65	0.269	21.01
PM6-Y6	0.3	20.94	0.062	91.21	1.74	3.61	0.258	21.92

[a] The d-spacing values are all calculated according to the Bragg's Law of $2dsin\theta = \lambda$; where $\lambda \approx 0.15418$ nm (Cu Kα); [b] Coherence length (CL) are calculated using the Scherrer equation: $CL = 2\pi K/\Delta q$; here, K is shape factor with the value of 0.89 typically, and Δq represents the full width at half maximum (FWHM) of the diffraction peak, respectively.

Table S6. The optimal photovoltaic parameters of studied OSCs under AM 1.5G Illumination (100 mW cm^{-2}).

Active layer	V_{oc} (V)	$^a J_{sc}$ (mA cm^{-2})	$^b Calc.J_{sc}$ (mA/cm^{-2})	$^a FF$ (%)	$^a PCE$ (%)
D18:NQF	**0.937**	**25.10**	**24.23**	**69.36**	**16.32**

[a]Optimal results are listed and the average parameters were calculated from 10 independent devices. [b]Current densities calculated from EQE curves.

4. ^{1}H, ^{13}C NMR and HRMS of compound 3, compound 4 and NQF
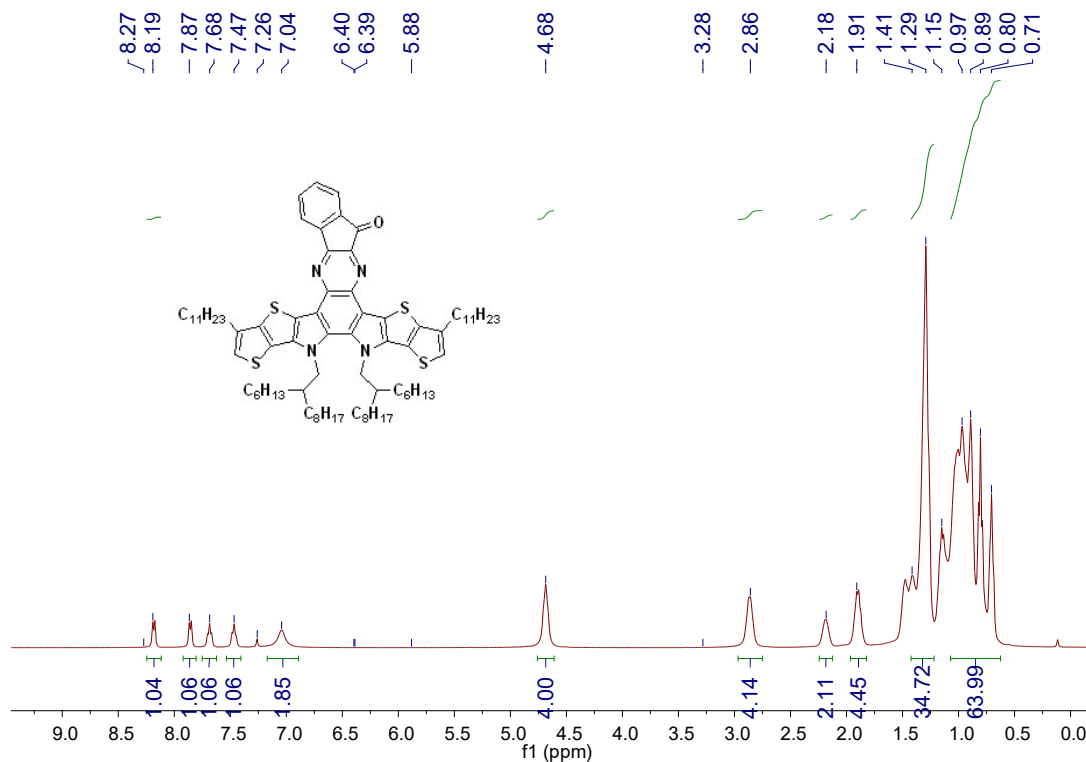
Figure S17. ^{1}H NMR spectrum of compound 3.
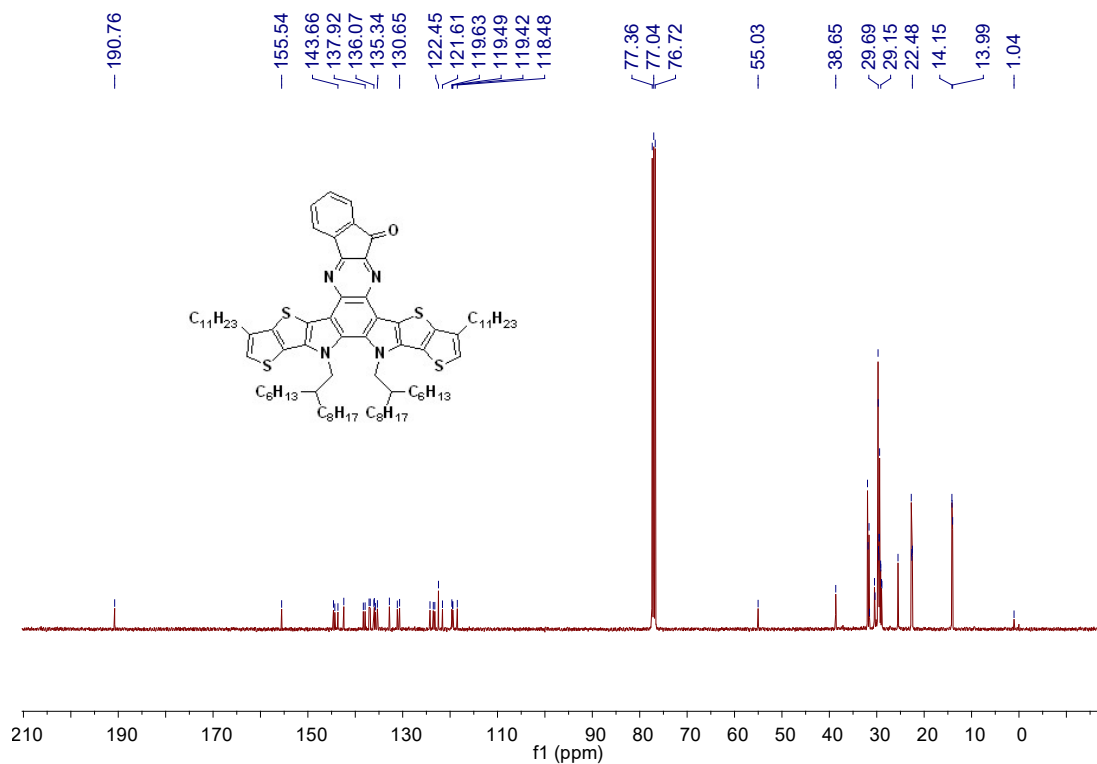
Figure S18. ^{13}C NMR spectrum of compound 3.
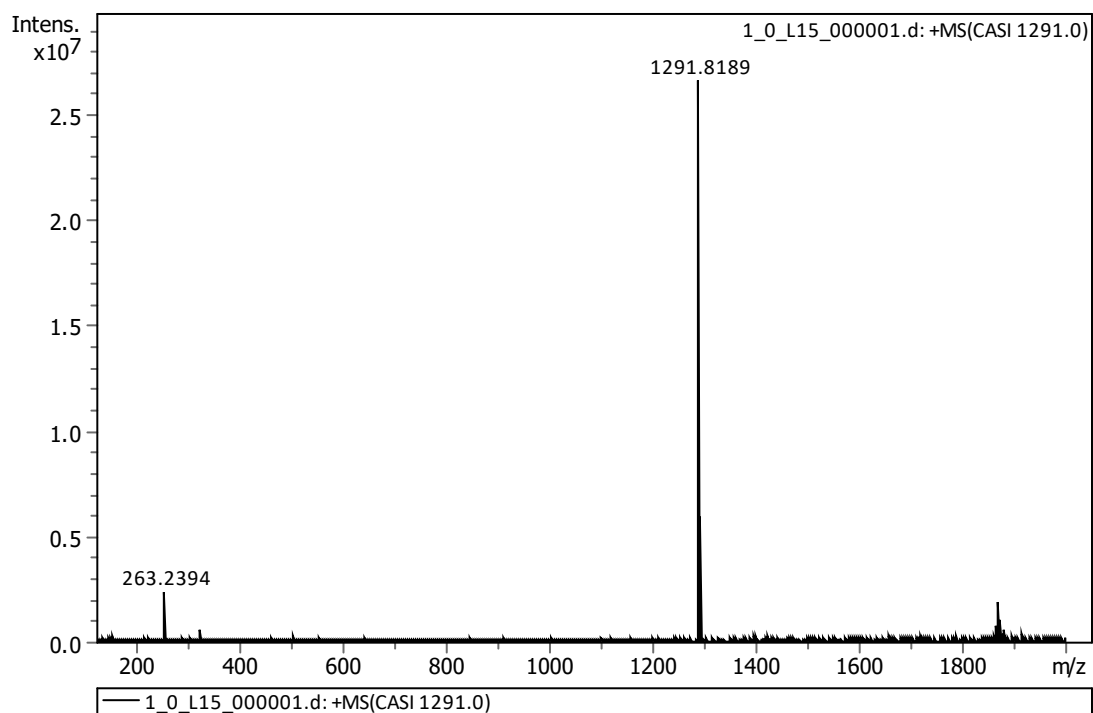
Figure S19. HRMS plot of compound 3.
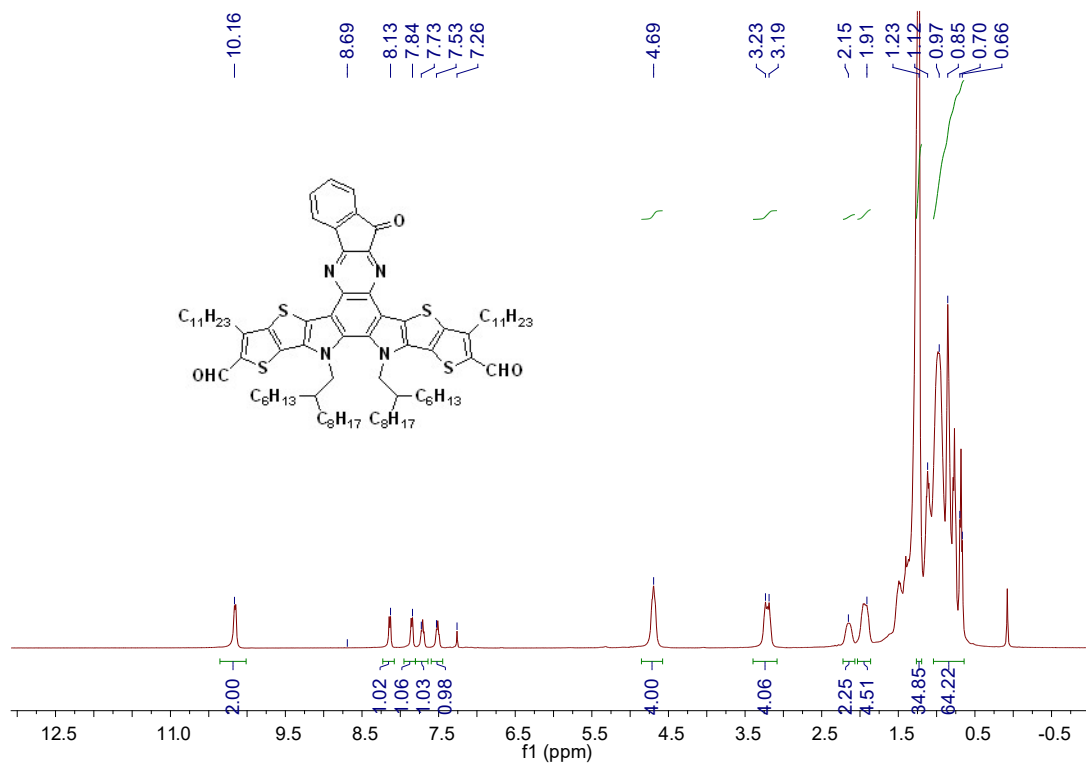
Figure S20. ^{1}H NMR spectrum of compound 4.
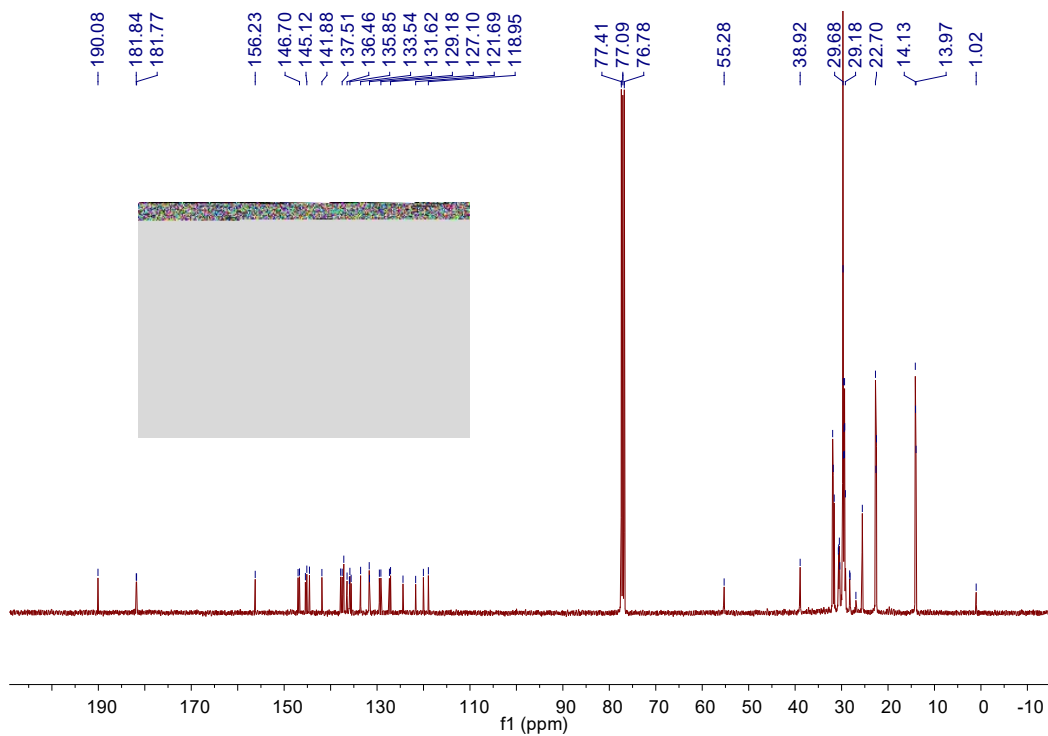
Figure S21. ^{13}C NMR spectrum of compound 4.
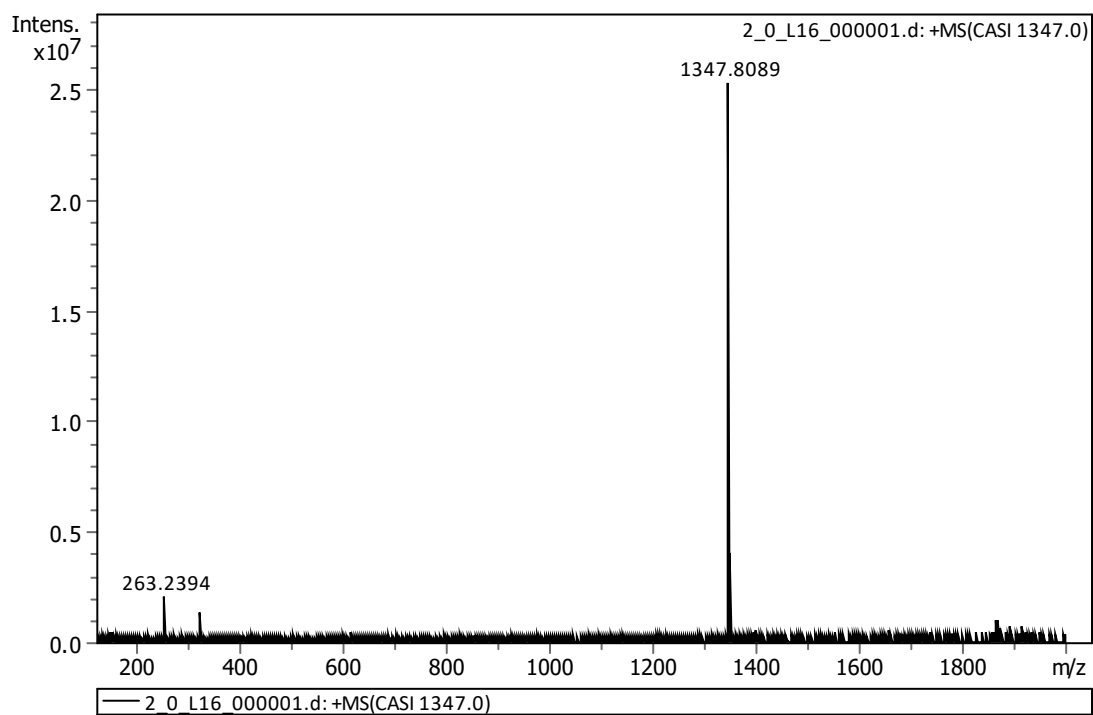
Figure S22. HR MS plot of compound 4.
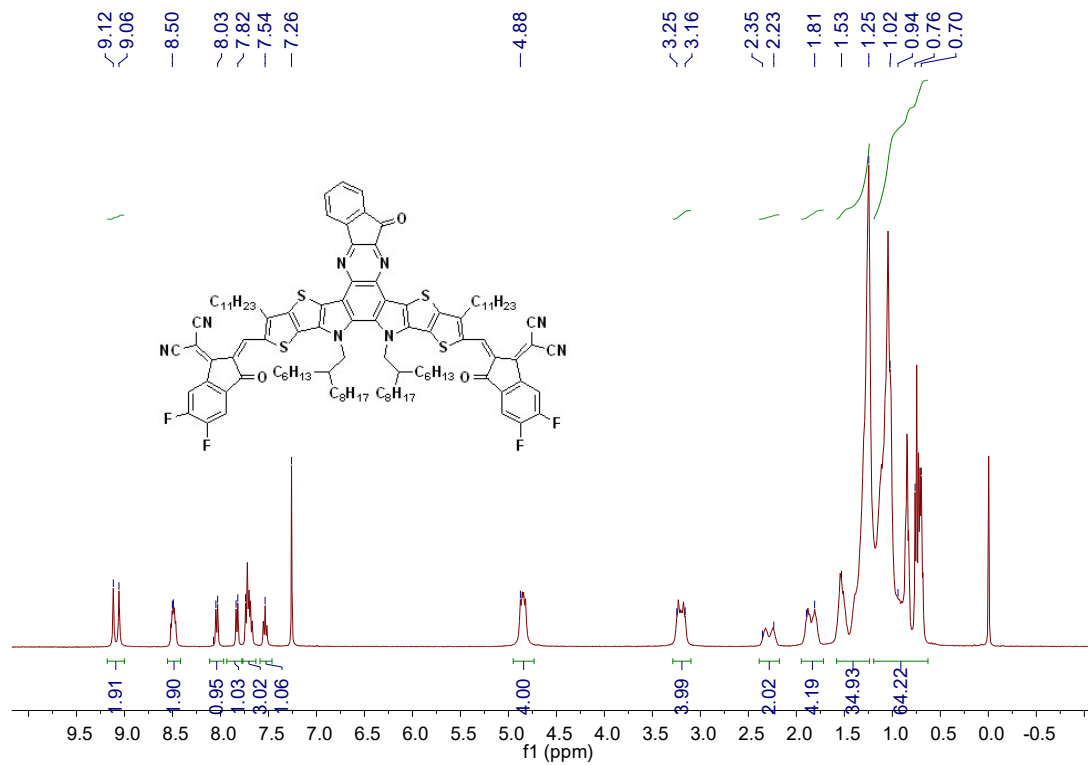
Figure S23. ^{1}H NMR spectrum of NQF.
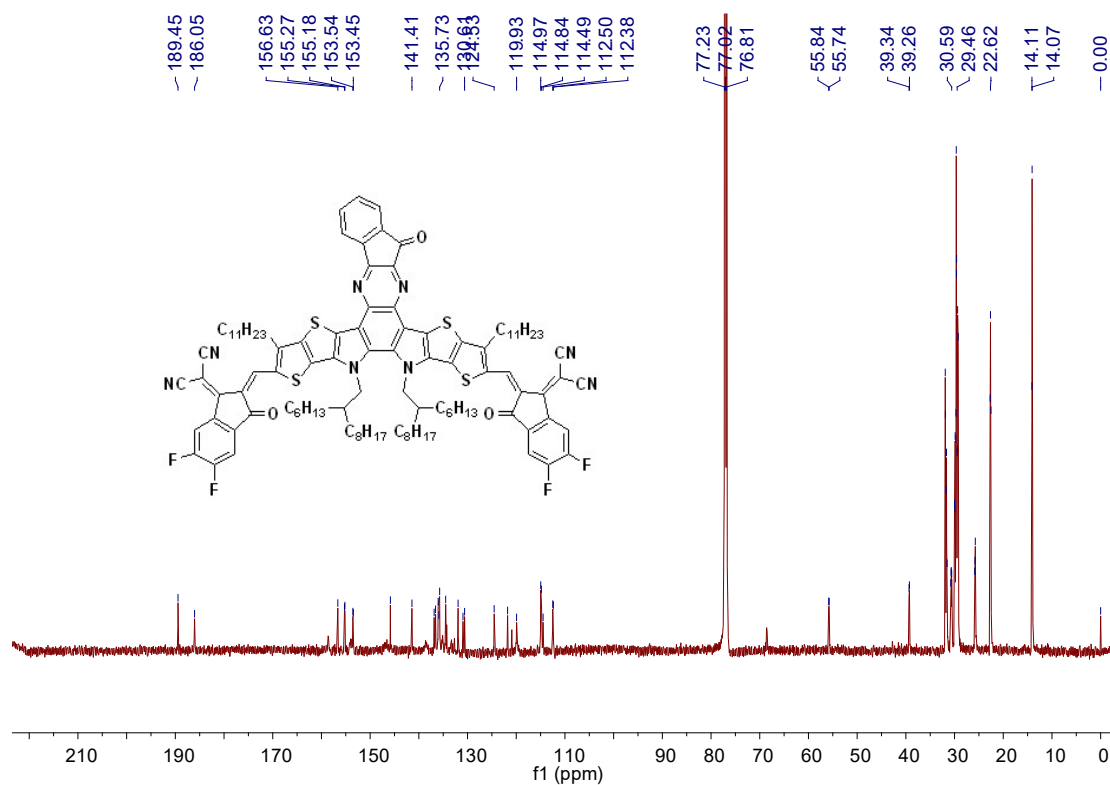
Figure S24. ^{13}C NMR spectrum of NQF.
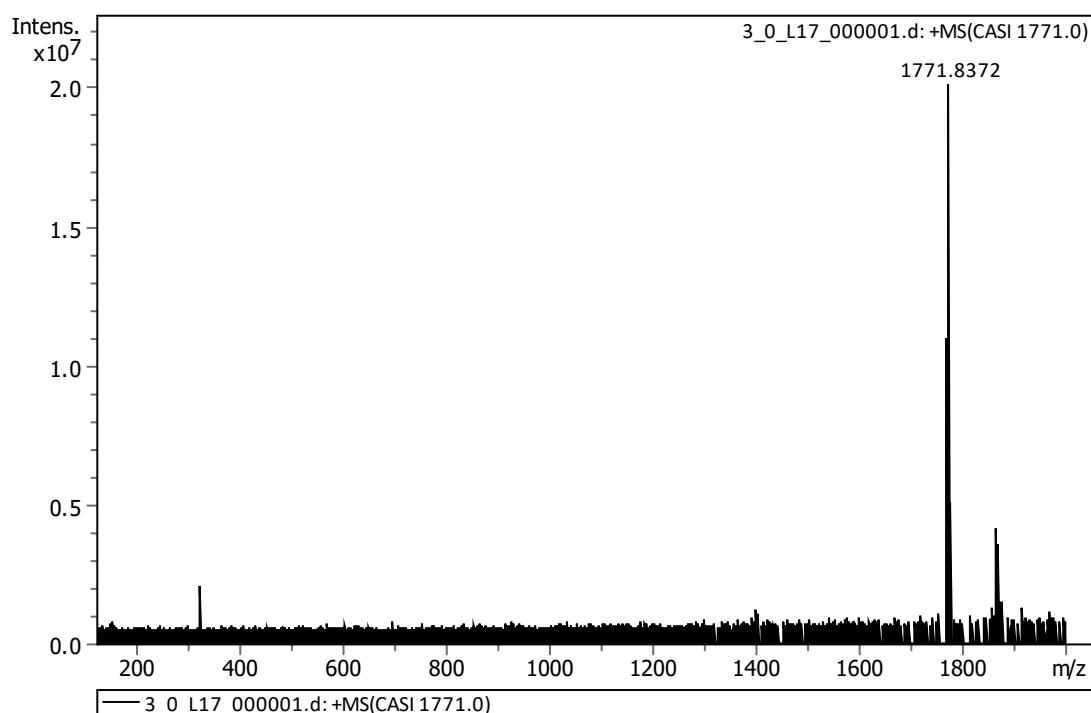
Figure S25. HR MS plot of NQF.

References

1. H. Q. Liu, M. Y. Li, H. B. Wu, J. Wang, Z. F. Ma and Z. Tang, *J. Mater. Chem. A*, 2021, **9**, 19770-19777.

2. N. An, Y. H. Cai, H. B. Wu, A. L. Tang, K. N. Zhang, X. T. Hao, Z. F. Ma, Q. Guo, H. S. Ryu, H. Y. Woo, Y. M. Sun and E. J. Zhou, *Adv. Mater.*, 2020, **32**, 2002122.

3. X. Liu, X. Du, J. Wang, C. Duan, X. Tang, T. Heumueller, G. Liu, Y. Li, Z. Wang, J. Wang, F. Liu, N. Li, C. J. Brabec, F. Huang and Y. Cao, *Adv. Energy Mater.*, 2018, **8**, 1801699.

4. D. Qian, Z. Zheng, H. Yao, W. Tress, T. R. Hopper, S. Chen, S. Li, J. Liu, S. Chen, J. Zhang, X.-K. Liu, B. Gao, L. Ouyang, Y. Jin, G. Pozina, I. A. Buyanova, W. M. Chen, O. Inganas, V. Coropceanu, J.-L. Bredas, H. Yan, J. Hou, F. Zhang, A. A. Bakulin and F. Gao, *Nat. Mater.*, 2018, **17**, 703-709.

5. D. Baran, T. Kirchartz, S. Wheeler, S. Dimitrov, M. Abdelsamie, J. Gorman, R. S. Ashraf, S. Holliday, A. Wadsworth, N. Gasparini, P. Kaienburg, H. Yan, A. Amassian, C. J. Brabec, J. R. Durrant and I. McCulloch, *Energy Environ. Sci.*, 2016, **9**, 378-3793.

6. S. Xie, Y. Xia, Z. Zheng, X. Zhang, J. Yuan, H. Zhou and Y. Zhang, *Adv. Funct. Mater.*, 2018, **28**, 1705659.

7. J. Liu, S. Chen, D. Qian, B. Gautam, G. Yang, J. Zhao, J. Bergqvist, F. Zhang, W. Ma, H. Ade, O. Inganas, K. Gundogdu, F. Gao and H. Yan, *Nat. Energy*, 2016, **1**, 16089.

8. Z. Fei, F. D. Eisner, X. Jiao, M. Azzouzi, J. A. Rohr, Y. Han, M. Shahid, A. S. R. Chesman, C. D. Easton, C. R. McNeill, T. D. Anthopoulos, J. Nelson and M. Heeney, *Adv. Mater.*, 2018, **30**, 1705209.

9. H. Lu, W. Liu, H. Jin, H. Huang, Z. Tang and Z. Bo, *Adv. Funct. Mater.* 2021, 2107756.

10. Y. Xie, W. Huang, Q. Liang, J. Zhu, Z. Cong, F. Lin, S. Yi, G. Luo, T. Yang, S. Liu, Z. He, Y. Liang, X. Zhan, C. Gao, H. Wu and Y. Cao, *ACS Energy Lett.*, 2019, **4**, 8-16.

11. C. Yao, B. Liu, Y. Zhu, L. Hong, J. Miao, J. Hou, F. He and H. Meng, *J. Mater. Chem. A*, 2019, **7**, 10212-10216.

12. Y. Cui, H. Yao, J. Zhang, T. Zhang, Y. Wang, L. Hong, K. Xian, B. Xu, S. Zhang, J. Peng, Z. Wei, F. Gao and J. Hou, *Nat. Commun.*, 2019, **10**, 2515.

13. Z. Luo, T. Liu, Y. Wang, G. Zhang, R. Sun, Z. Chen, C. Zhong, J. Wu, Y. Chen, M. Zhang, Y. Zou, W. Ma, H. Yan, J. Min, Y. Li and C. Yang, *Adv. Energy Mater.*, 2019, **9**, 1900041.

14. S. Liu, J. Yuan, W. Deng, M. Luo, Y. Xie, Q. Liang, Y. Zou, Z. He, H. Wu and Y. Cao, *Nat. Photonics*, 2020, **14**, 300-305.

15. W. Liu, S. Sun, L. Zhou, Y. Cui, W. Zhang, J. Hou, F. Liu, S. Xu, X. Zhu, *Angew. Chem. Int. Ed.*, **2022**, e202116111.

16. H. Lu, H. Jin, H. Huang, W. Liu, Z. Tang, J. Zhang and Z. Bo, *Adv. Funct. Mater.*, 2021, **31**, 2103445.

17. Y. Cui, H. Yao, J. Zhang, K. Xian, T. Zhang, L. Hong, Y. Wang, Y. Xu, K. Ma, C. An, C. He, Z. Wei, F. Gao and J. Hou, *Adv. Mater.*, 2020, **32**, 1908205.

18. S. Li, L. Zhan, Y. Jin, G. Zhou, T.-K. Lau, R. Qin, M. Shi, C.-Z. Li, H. Zhu, X. Lu, F. Zhang and H. Chen, *Adv. Mater.*, 2020, **32**, 2001160.